OTC 23714

Petermann Ice Island 'A' Survey Results, Offshore Labrador

E. Julie Halliday, C-CORE & Memorial University, Tony King and Pradeep Bobby, C-CORE, Luke Copland, University of Ottawa, and Derek Mueller, Carleton University.

Abstract

In August 2010 a 265 km^2 ice island calved from the Petermann Glacier in northern Greenland. Soon after the initial calving event the mass broke into several pieces, some of which exited Baffin Bay and drifted south toward the Labrador coast. By June 2011 PII-A, a large fragment of the initial Petermann Ice Island, was situated offshore Labrador and in one week it had moved 225 km down the coast. Concern arose that if PII-A continued its trajectory it could reach the Grand Banks by August 2011, posing a potential risk for existing infrastructure in the offshore region of Newfoundland. To properly assess the potential risk a realistic estimate of ice mass was necessary. This in turn required field measurements of the ice islands thickness.

A three-day field program was carried out on the Petermann Ice Islands, PII-A and PII-A-a, from June 17-19, 2011. At this time PII-A and PII-A-a were situated offshore Labrador, Canada, approximately 100 km northeast of the town of Rigolet. Geophysical survey methods, including Ground Penetrating Radar (GPR) and Seismic Reflection, were used to identify the base of the islands and obtain ice thickness measurements at various locations. Eight satellite tracking beacons were deployed on PII-A and one was deployed on PII-A-a. Ablation data, photographs and video footage were also obtained during the program. On July 22, 2011, PII-A was revisited while it was situated off the southern Labrador coast. GPR measurements were acquired at the pre-existing stations; the measurements allowed for deterioration rates due to surface and basal melting to be calculated for PII-A. Results of the field measurements indicate that ice thickness varied between 50 to 80 m on PII-A; the thickness of PII-A-a was 30 m at a single survey location. Surface melt rates of 2.7-6.3 cm day^{-1} were observed over a 1-day period in June. For the 35-day period between June and July visits, average surface and basal melt of 5.0 cm day^{-1} and 3.4 cm day^{-1}, respectively, were calculated.

Introduction

With the advancement of exploration into high-latitude areas such as offshore Greenland, and the Beaufort and Chukchi seas, the occurrence of large floating ice masses in close proximity to petroleum infrastructure may become more commonplace in the near future. The risks inherent to operating in ice-laden environments include ice-impact with structures at the sea surface such as gravity-based platforms, as well as those on the seabed such as risers and pipelines. There is also the high expense and difficulty associated with tracking large quantities of ice fragments, which in turn increases the complexity and cost of ice management strategies. It is therefore important to understand the characteristics and drift patterns of ice islands and other large masses of ice (e.g., multiyear ice floes) to minimize the risks associated with operating in their vicinity. This paper presents results from a field study of an ice island that was situated in the offshore region of Labrador during 2011. Ice islands are unique features to the Arctic and are formally defined as "*A large piece of floating ice protruding about 5 m above sea level, which has broken away from an Arctic ice shelf. They have a thickness of 30-50 m and an area of from a few thousand square metres to 500 sq. km or more. They are usually characterized by a regularly undulating surface giving a ribbed appearance from the air*" (Service and Canada, 2005). Results from the study are relevant for Arctic and sub-Arctic operators of today and tomorrow.

On August 4, 2010, a 253 +/- 17 km^2 ice island calved from the Petermann Glacier in northern Greenland (Figure 1) (Falkner et al., 2011). The calving event occurred along a preexisting rift and marked the largest annual change in mass for a single Greenland glacier over a 10-year observation period (Box and Decker, 2011; Nick et al., 2012). In September 2010, while in

Nares Strait, the island split into two pieces: Petermann Ice Islands A and B (PII-A, PII-B). Over the next eight months PII-A drifted south, ending up off the northern coast of Labrador by May 2011 (Figure 2). By early June 2011 the 12 km by 6 km ice island PII-A was situated in the offshore region of Labrador and in one week moved 225 km southeast along its coast. The proximity of this ice mass to the coastline presented an opportunity to conduct helicopter-assisted fieldwork over three days. An opportunistic revisit to the ice island was made in July via ship-support. The primary aim of the fieldwork was to determine the thickness of the ice island, so that an accurate estimate of its mass could be calculated. The mass estimate is in turn useful for computations of ice loading on structures and determination of ice management schemes. Geophysical means were used to measure the ice thickness at various points on the ice island. Other data collected included measurements of surface melt, video footage and monitoring of ice island drift with GPS tracking beacons.

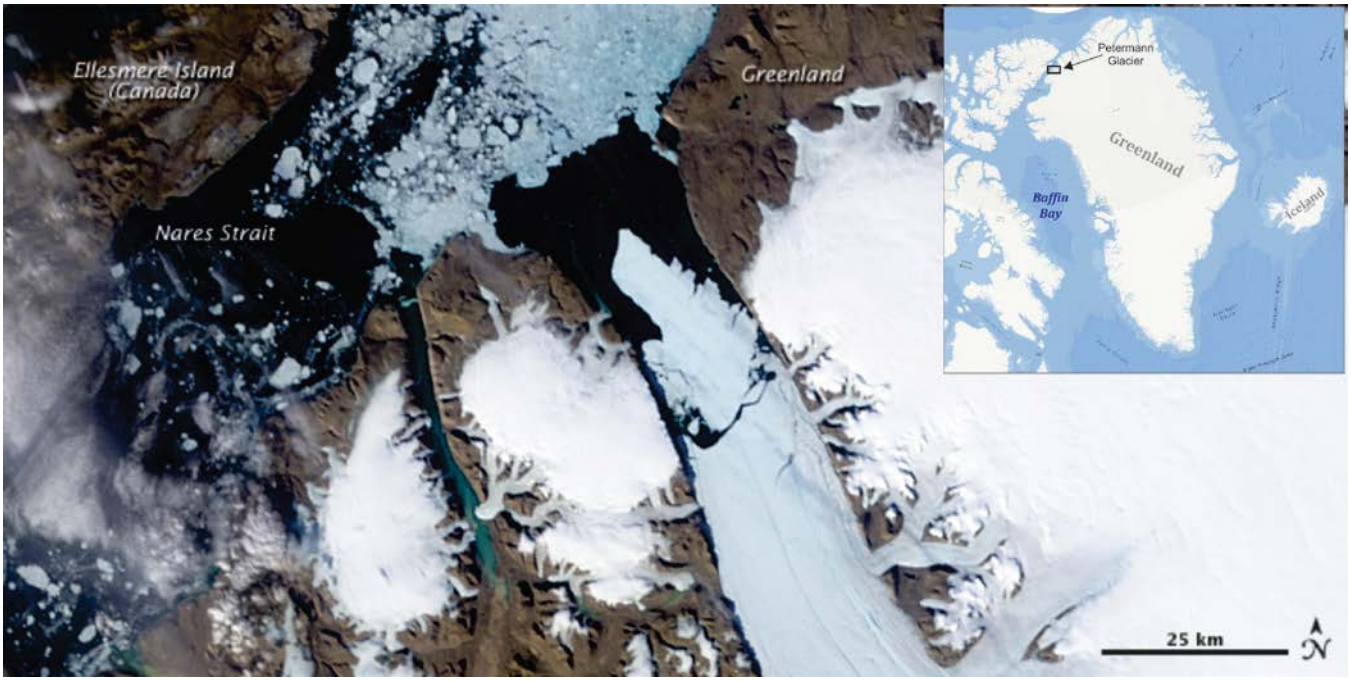

Figure 1. MODIS Terra optical satellite image of the Petermann Glacier in northeastern Greenland acquired at 18:05 UTC on August 5th, 2010 (Allen and Simmon, 2010). On August 4th, 2010 a calving event occurred which produced the 253 km^2 Petermann Ice Island (Falkner et al., 2011). The ice island subsequently exited the fjord and split into two large fragments, PII-A and PII-B.

Methods

Three days of helicopter-based fieldwork were conducted on ice islands PII-A and PII-A-a on June 17-19, 2011, while they were situated in the offshore region of Labrador. In the days leading up to this fieldwork, PII-A split into two ice islands: PII-A and PII-A-a (Figure 2). Both of these ice islands were visited during the June field program, which consisted of three trips from a staging area in Rigolet, Labrador. Data was collected at fourteen stations over the course of the three days (Figure 3, Table 1). Survey site locations were chosen with the objective of sampling the long and short axis of the ice island. The ability of the helicopter to land also played a role in site selection. Once landed a level site, away from streams or ponds, was sought for installation of instruments. Another day of ship-supported fieldwork was conducted on July 22, 2011, from Canadian Coastguard Ship Amundsen, during which PII-A was visited and data were collected at four of the original stations (Table 1).

Ground Penetrating Radar (GPR) data were collected at nine stations: eight on PII-A and one on PII-A-a (Table 1, Figure 4). The GPR system consisted of a monopulse transmitter based on the design of (Narod and Clarke, 1994), resistively-loaded dipoles, and an air wave triggered Tektronix THS720A digital oscilloscope. A centre-frequency of 10 MHz was used for the measurements, and the receiver and transmitter arms were laid parallel to each other on the ice surface at a separation distance of ~10 m. Traces were stacked 8 times prior to recording, and a low pass 15 MHz filter (Mini-Circuits BLP-15) was used to remove high frequency noise. Ice thicknesses were determined from the peak of the air wave to the peak of the bed wave, using a radio-wave velocity of 0.168 m ns^{-1} appropriate for temperate ice (Macheret et al., 1993).

Reflection seismic data were acquired at Station 12 (Table 1, Figure 4). The source-receiver setup consisted of a 4.5 kg sledgehammer struck on a metal plate and a 6-channel geophone array with 5 m receiver spacing. The geophones were installed in tapered holes drilled in the ice surface with an electric drill. Source to first-receiver offset was 8 m, yielding a far-offset of 33 m. A Geometrics Stratavisor seismograph was used to record the seismic reflection data. Ten shots were recorded and stacked to increase the signal to noise ratio. The record length and sampling frequency were 200 ms and 0.250 ms,

respectively, yielding a Nyquist frequency of 2000 Hz. Seismic data were processed with Globe *Claritas* software; processing included trace editing, bandpass filtering and automatic gain control (AGC) application.

Five ablation stakes were installed on the ice islands: four on PII-A and one on PII-A-a (Table 1, Figure 4). Ablation stakes consisted of 3 m long, 2.5 cm internal diameter, grey PVC pipes which were installed in the ice surface to a depth of ~2.60 m using a manually operated Kovacs ice auger. The proportion of the stake above the ice surface was measured. Satellite tracking beacons were deployed at nine stations, eight on PII-A and one on PII-A-a.

A Trimble R7 differential GPS (dGPS) system was set up and run at five stations for ~30-60 minutes to determine surface elevation, and therefore freeboard. The dGPS data were processed using the online precise point positioning service offered by Natural Resources Canada (http://www.geod.nrcan.gc.ca/products-produits/ppp_e.php), which is based on a reconstruction of satellite orbital parameters and removes the need for a fixed base station. The draft at each dGPS station was then determined by subtracting the elevation from total thickness determined by GPR measurements at the stations. Tidal corrections were not applied to the elevation data, so the resulting draft calculations may be off by up to +/- 1 m (based on tidal observations from Nain, Labrador; Fisheries and Oceans Canada, http://www.tides.gc.ca).

Numerous photos were taken with a digital SLR camera to document ice conditions while on the ice island and while airborne from the helicopter. Video footage was taken during a flight around the perimeter of ice island PII-A.

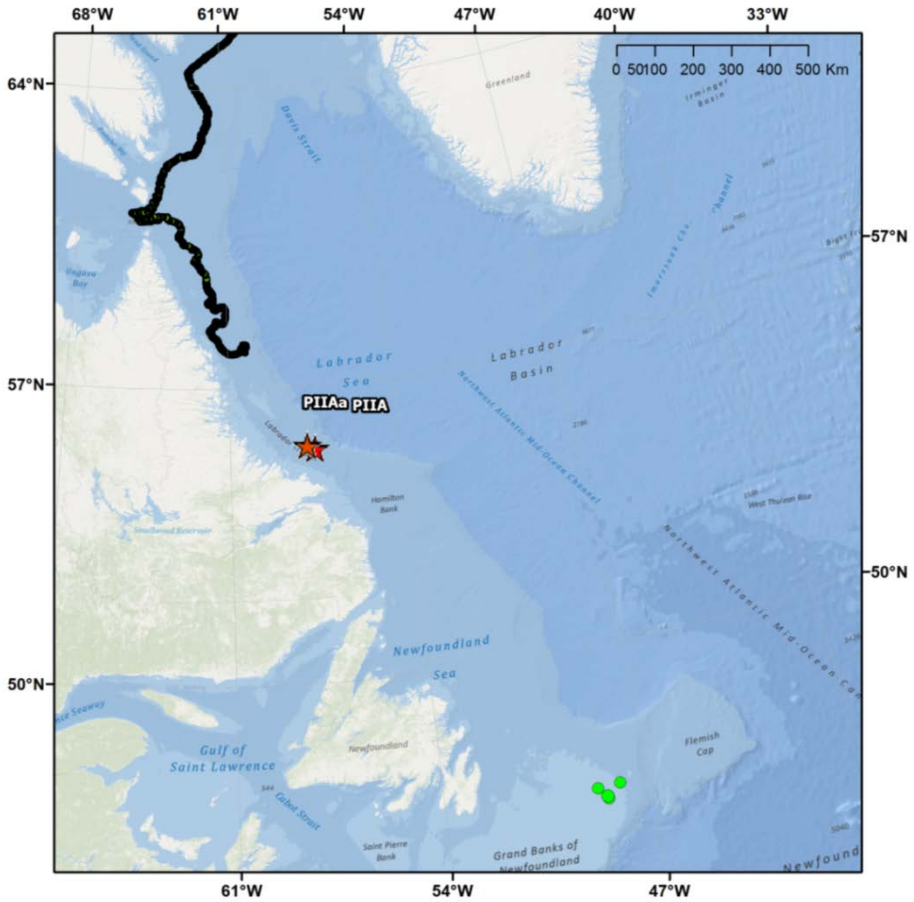

Figure 2. Black line shows the southward movement of PII-A from September 2010 to May 2011. Red stars indicate the position of PII-A and PII-A-a on June 15, 2011. Green circles show the location of oil production facilities in the offshore of Newfoundland. Position data from drifter buoy 47557 available at http://www.sailwx.info (LLC, 2012).

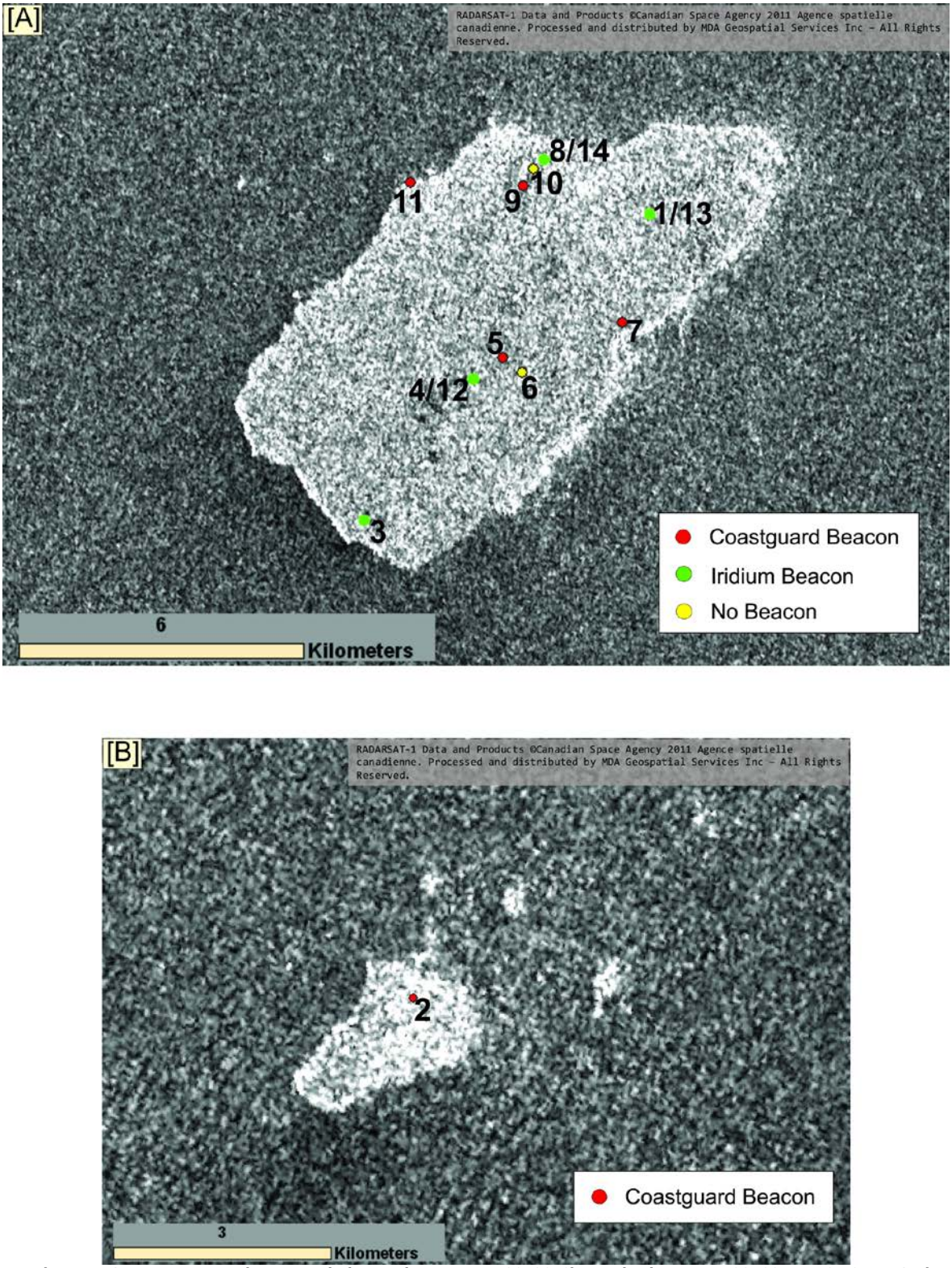

Figure 3. Radarsat-1 Scansar narrow beam-mode image (Image ID: N0610679) acquired on June 22, 2011 at 21:27 UTC showing the ID and location of stations on PII-A [A] and PII-A-a [B], offshore Labrador, June 2011 (Agency, 2011). In this image, the geographic position of station 5 was -55.378946W, 54.880192N, while station 2 was at -57.671549W, 55.311964N.

Table 1. Summary of data collected on PII-A and PII-A-a ice islands, by station number. Bracketed numbers in first column indicate stations that were visited a second time, a day after the first visit.

Station	Ice Island	Date	Time (AST) (-3hrs from UTC)	Beacon IMEI #	Ablation stake above ice (m)		Ice Thickness (m)			Differential GPS surface elev. (m)
					Visit 1 (June 17-19)	Visit 2 (July 22)	GPR		Seismic	
							June 17-19	July 22		
1	PII-A	17/06/2011	16:00	3002 340 1003 3940	0.28	1.98	52.3	50.4	-	8.35
2	PII-A-a	17/06/2011	17:40	3000 340 1345 3190	0.12		30.5		-	7.25
3	PII-A	18/06/2011	11:00	3002 340 1003 5940	0.345	2.15	81.2	78.2	-	12.16
4	PII-A	18/06/2011	12:20	3002 340 1095 8690	0.36	2.02	72.3	68.4	-	10.12
5	PII-A	18/06/2011	14:20	3000 340 1345 8130	-		75.7	73.2	-	-
6	PII-A	18/06/2011	14:40	-	-		66.5		-	-
7	PII-A	18/06/2011	15:20	3000 340 1314 9880	-		-		-	-
8	PII-A	18/06/2011	15:30	3002 340 1095 5700	0.41	2.15	48.3	45.4	-	8.44
9	PII-A	18/06/2011	16:45	3000 340 1345 3240	-		50.9		-	-
10	PII-A	18/06/2011	17:10	-	-		48.7		-	-
11	PII-A	18/06/2011	17:35	3002 340 1095 9530	-		-		-	-
12 (4)	PII-A	19/06/2011	15:15	3002 340 1095 8690	0.405				70.2	
13 (1)	PII-A	19/06/2011	15:21	3002 340 1003 3940	0.343					
14 (8)	PII-A	19/06/2011	15:41	3002 340 1095 5700	0.437					

Results

Thickness.

Ground Penetrating Radar.

GPR measurements were collected at nine stations during the June fieldwork; GPR was acquired at four of the nine stations during the July visit (Table 1). Reflections at the ice-water interface were strong in all traces, likely due to the strong dielectric contrast between the base of the ice island and underlying ocean water (Figure 6). A secondary reflection was often observed in the GPR traces equidistant from the first, which is interpreted as a multiple. The maximum thickness measured from GPR data was 81.2 m recorded at Station 3 on PII-A; the minimum measured thickness was 30.5 m on PII-A-a (Figure 4, Table 1).

Seismic.

Seismic data was collected at Station 12 (repeat of Station 4) during the June fieldwork. The processed shot gather is depicted in Figure 6. A strong, laterally continuous negative-impedance reflection is observed at 46.79 ms at channel 1 and can be traced across the section to channel 6. This event is interpreted as the ice-water interface due to its negative polarity

(i.e., high to low sound velocity associated with ice to water transition will generate negative impedance contrast). Using a p-wave velocity of 3000 m s^{-1} for ice (calculated from the direct arrival), yields an ice thickness of 70.2 m at station 12. This is within ~2 m of the thickness measured by GPR at this site (72.3 m).

Draft.

The surface elevation of the ice island was determined at five stations (1-4 and 8) using dGPS measurements collected at these stations during the June fieldwork. Ice island thickness, elevation and draft are listed in Table 2.

Table 2. Thickness, elevation and calculated draft at stations on PII-A and PII-A-a based on field measurements made in June 2011. Total thickness values are based on GPR measurements. Thickness value in brackets at station 4 is based on reflection seismic measurement. Surface elevations are based on dGPS measurements.

Station	Total Thickness (m)	Surface Elevation (m)	Draft(m)
1	52.3	8.35	43.95
2	30.5	7.25	23.25
3	81.2	12.16	69.04
4	72.3 (70.2)	10.12	62.18
8	48.3	8.44	39.86

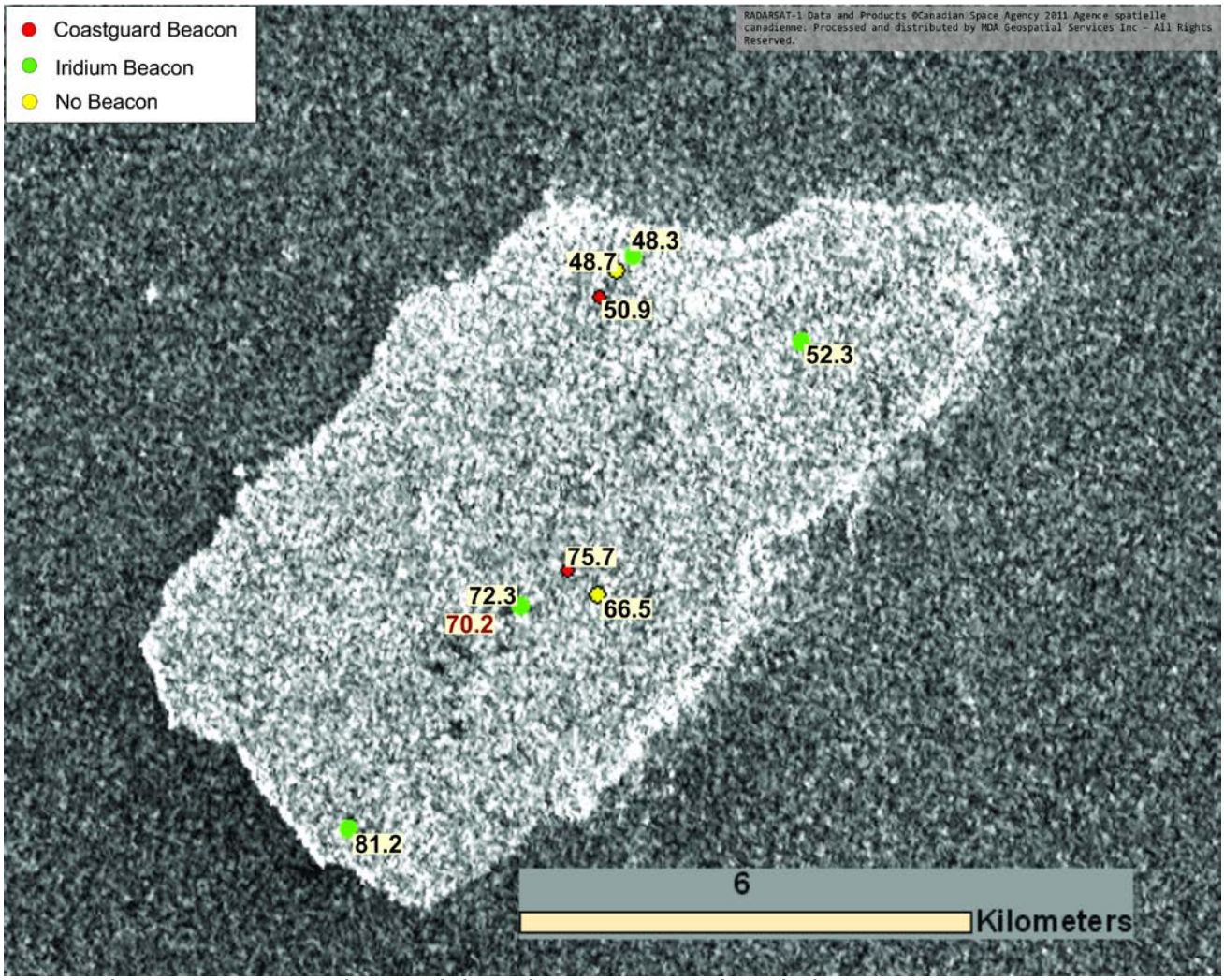

Figure 4. Radarsat-1 Scansar narrow beam-mode image (Image ID: N0610679) acquired on June 22, 2011 at 21:27 UTC showing PII-A. Point thicknesses (in meters) of the ice island, as measured from GPR and seismic reflection measurements, are shown. GPR thicknesses are based on a radio wave velocity of 0.168 m ns^{-1} in ice and depicted in black font. Thickness calculated from seismic reflection data is depicted in red font and based on a p-wave velocity of 3000 m s^{-1} for ice.

Melt Rates.

Three of the five ablation stakes were remeasured during the June fieldwork (the next day after emplacement), and four were remeasured during July fieldwork. Table 4 summarizes the results, including the surface melt and bottom melt

calculated from the difference between the June and July GPR thickness measurements. The distribution of these values on PII-A is shown in Figure 7. The largest change in thickness occurred toward the centre of PII-A at Station 4, over 2 km from its edge; the smallest change occurred >1.5 km from its edge at Station 1. The total change in thickness at Station 5 was 2.5 m. Station 5 is approximately 750 m away from Station 4, which experienced a 4.0 m decrease in thickness. Surface melt on PII-A varied from 1.66-1.80 m (4.9-5.3 cm day^{-1}), with an average surface melt of 1.72 m (5 cm day^{-1}). Bottom melt varied from 0.2-2.3 m (5.7-6.8 cm day^{-1}), with an average of 1.23 m (3.4 cm day^{-1}). Station 1 experienced the least amount of bottom melt (0.2 m) and the smallest overall change in thickness (1.9 m).

Table 3. Thickness change from June to July visits at stations on PII-A, as derived from GPR measurements (see Table 1). Surface melt equals the change in ablation stake height from initial installation to the height at July visit. Bottom melt is the difference between the thickness change and surface melt. Time elapsed between visits was calculated in hours and the values were used to calculate daily melt rates.

Station	Thickness Change (m)	Total Surface Melt (m)	Surface Melt (cm day^{-1})	Bottom Melt (m)	Bottom Melt (cm day^{-1})
1	1.9	1.7	4.9	0.2	5.7
3	3.0	1.80	5.3	1.2	3.5
4	4.0	1.66	4.9	2.3	6.8
5	2.5	-	-	-	-
8	2.9	1.74	5.1	1.2	3.5

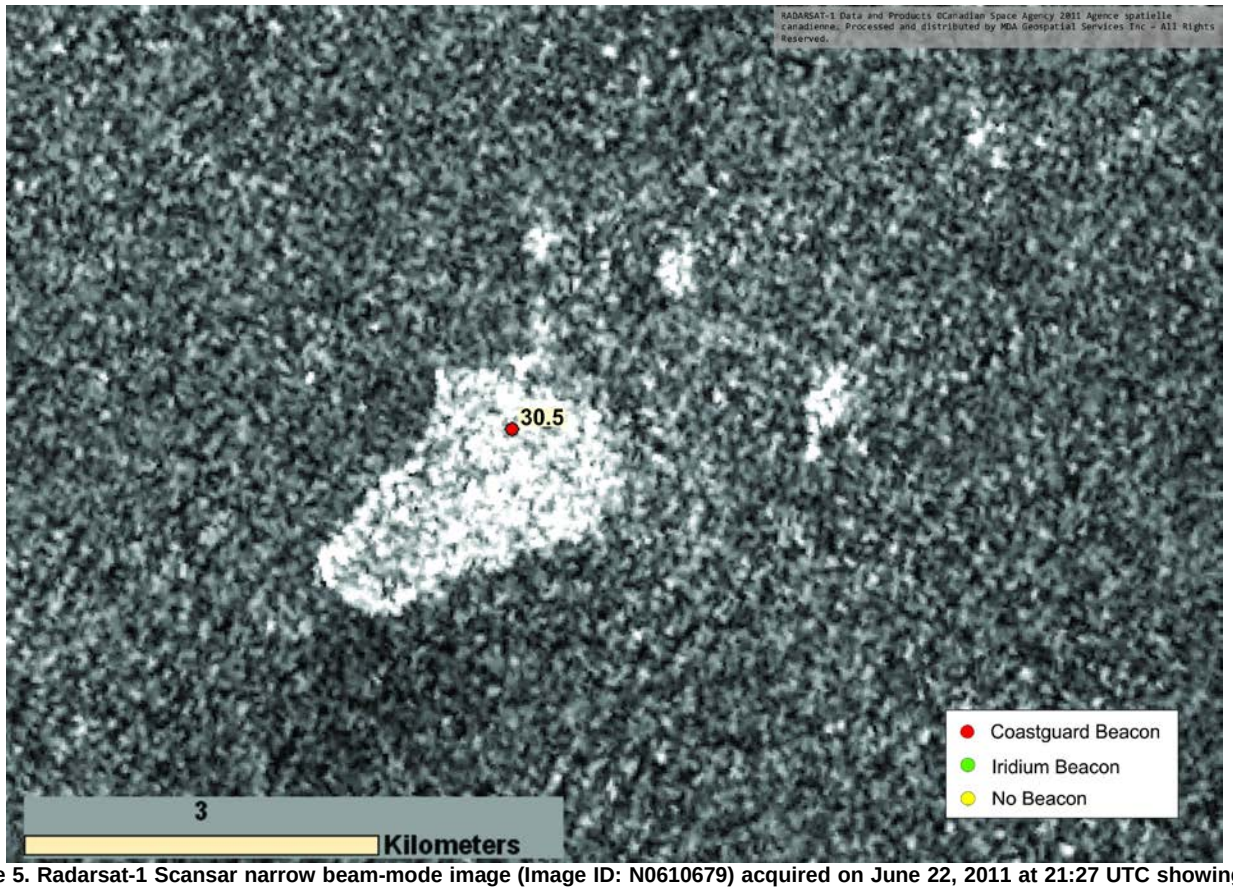

Figure 5. Radarsat-1 Scansar narrow beam-mode image (Image ID: N0610679) acquired on June 22, 2011 at 21:27 UTC showing PII-A-a. The point thickness (in meters) of PII-A-a on June 17, 2011, from GPR measurements is shown. GPR thickness is based on a radio wave velocity of 0.168 m ns^{-1} in ice.

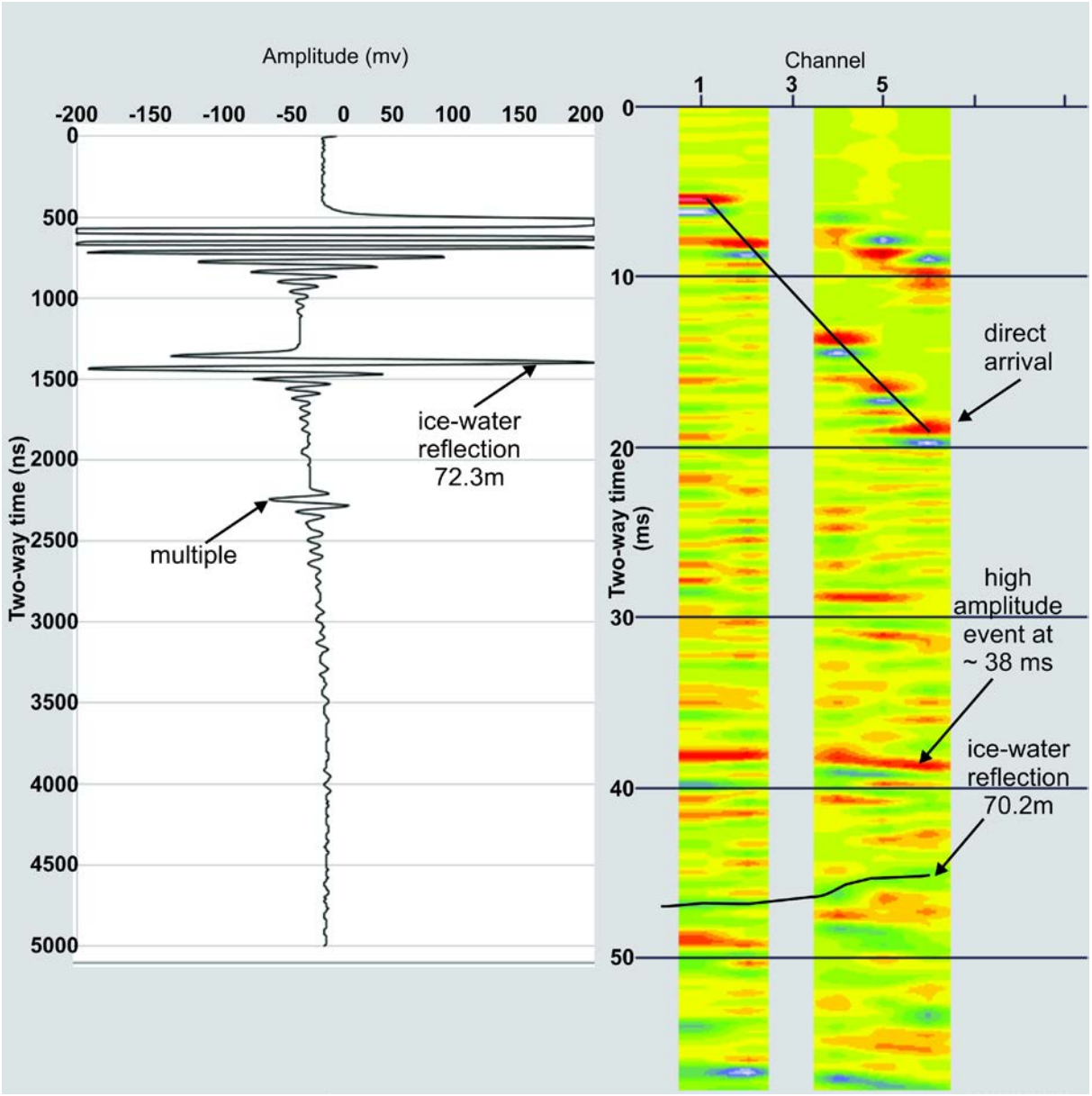

Figure 6. GPR (left) and seismic data (right) collected at Station 4/12 on PII-A during June 2011 fieldwork. GPR data indicate an ice thickness of 72.3 m, seismic data yield an ice thickness of 70.2 m. Seismic plot colours represent true amplitude, where red is positive and blue is negative amplitude, respectively. For GPR data the ice thickness was calculated from the two-way travel time between the airwave and the bottom reflection. For seismic data, thickness was calculated from the two-way travel time of the ice-water reflection using a p-wave velocity of 3000 m s^{-1} calculated from the direct arrival.

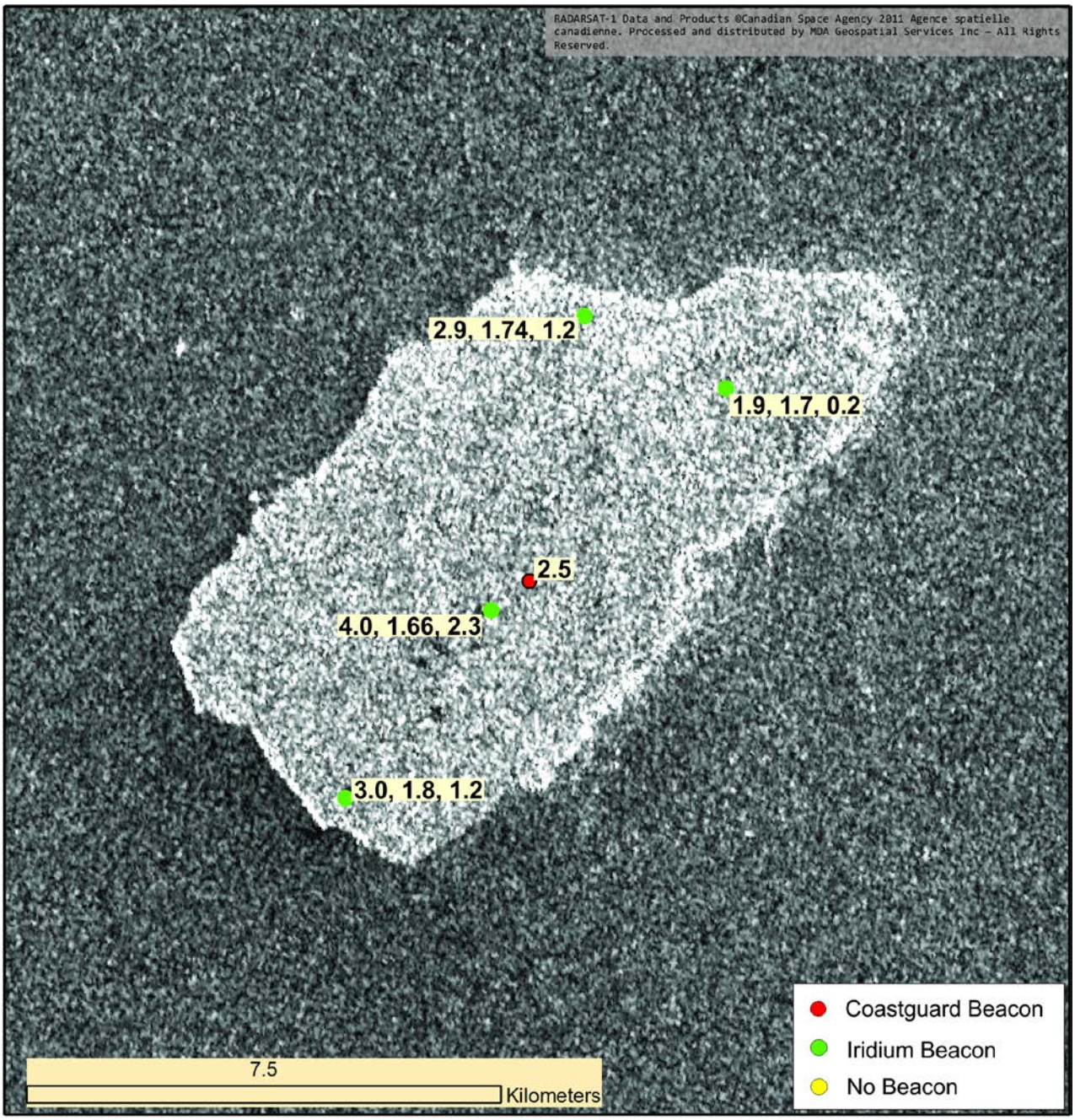

Figure 7. Radarsat-1 Scansar narrow beam-mode image (Image ID: N0610679) acquired on June 22, 2011 at 21:27 UTC showing PII-A. From left to right the values indicate: total thickness change, surface melt and bottom melt observed at stations on PII-A from June – July 2011. Total thickness change calculated from difference between June and July GPR measurements. Surface melt calculated from change in height of ablation stakes between June and July. Bottom melt calculated from difference between total thickness change and surface melt.

Field Observations.

Numerous meltwater features were observed on the ice surface including ponds, rivers, streams and cryoconite holes (Figure 8, Figure 9). Approximate dimensions of the features were as follows: ponds were between 200-400 m long, 100-200 m wide and <5 m deep; rivers were kilometers long and <5 m wide and deep; streams were <1 km in length, 1-1.5 m wide and <1 m deep; cryoconite holes were 10-50 cm in diameter and between 20-50 cm deep. In June, the surface of the ice had large crystals and slush in places (Figure 9). A band of frozen slush was generally present on the edge of meltwater features. Numerous icebergs were observed around the periphery of PII-A and PII-A-a that had calved from these ice islands (Figure 10). Seals (>1000) were found on top of both ice islands, in the adjacent ocean and on top of peripheral icebergs (Figure 10). Seals were absent from the center of PII-A, although on PII-A-a a few seals were observed >1.5 km from the islands edge. Surface striations and re-frozen crevasses were observed on both PII-A and PII-A-a. Ridges of varying height were present on PII-A and PII-A-a (Figure 9, Figure 10), with a maximum height of ~15 m above the surrounding ice.

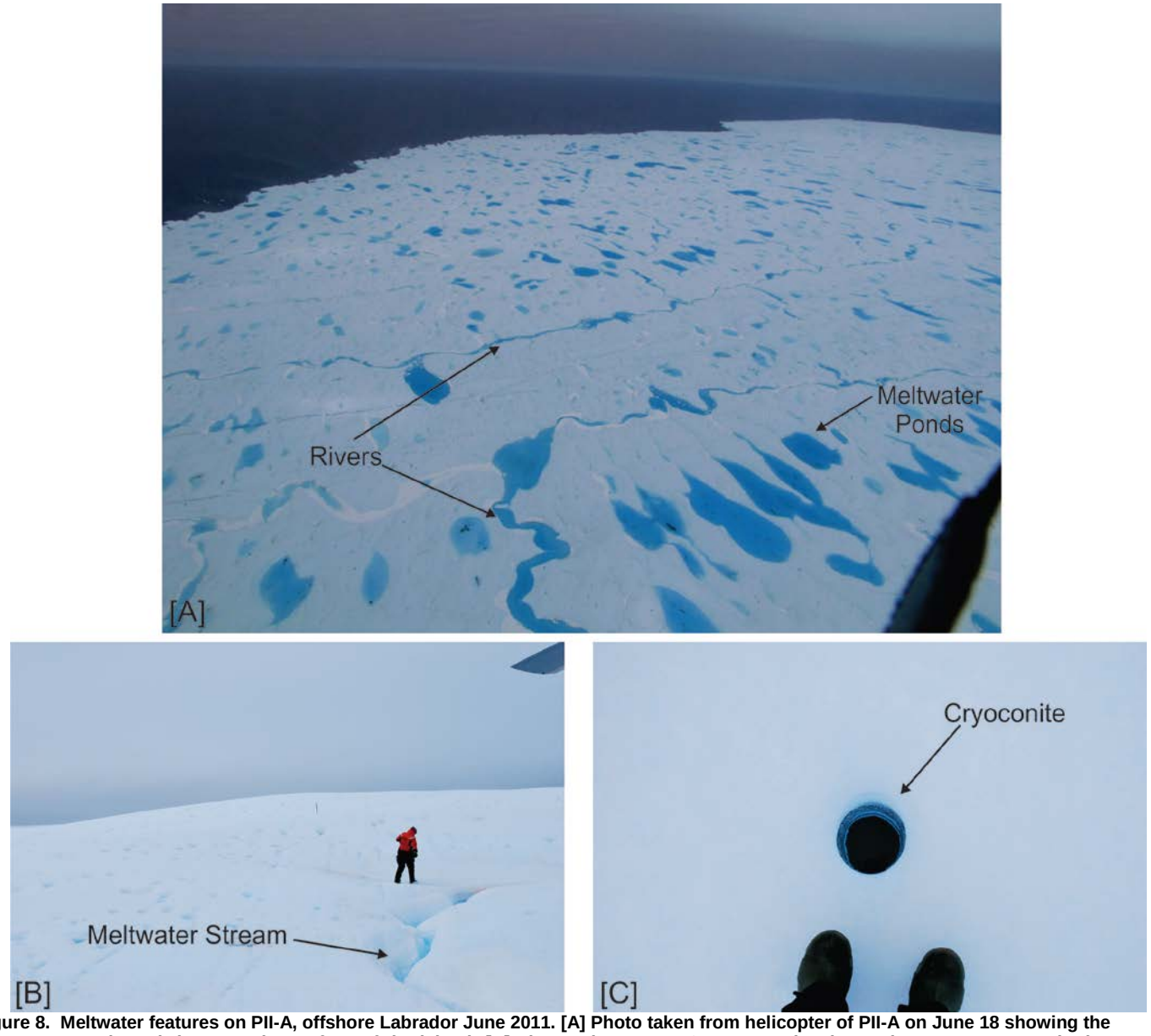

Figure 8. Meltwater features on PII-A, offshore Labrador June 2011. [A] Photo taken from helicopter of PII-A on June 18 showing the numerous ponds and rivers on the surface of the island; [B] photo taken June 19 on PII-A showing meltwater stream on the ice surface; [C] photo taken on June 17on PII-A showing cryoconite on the ice surface.

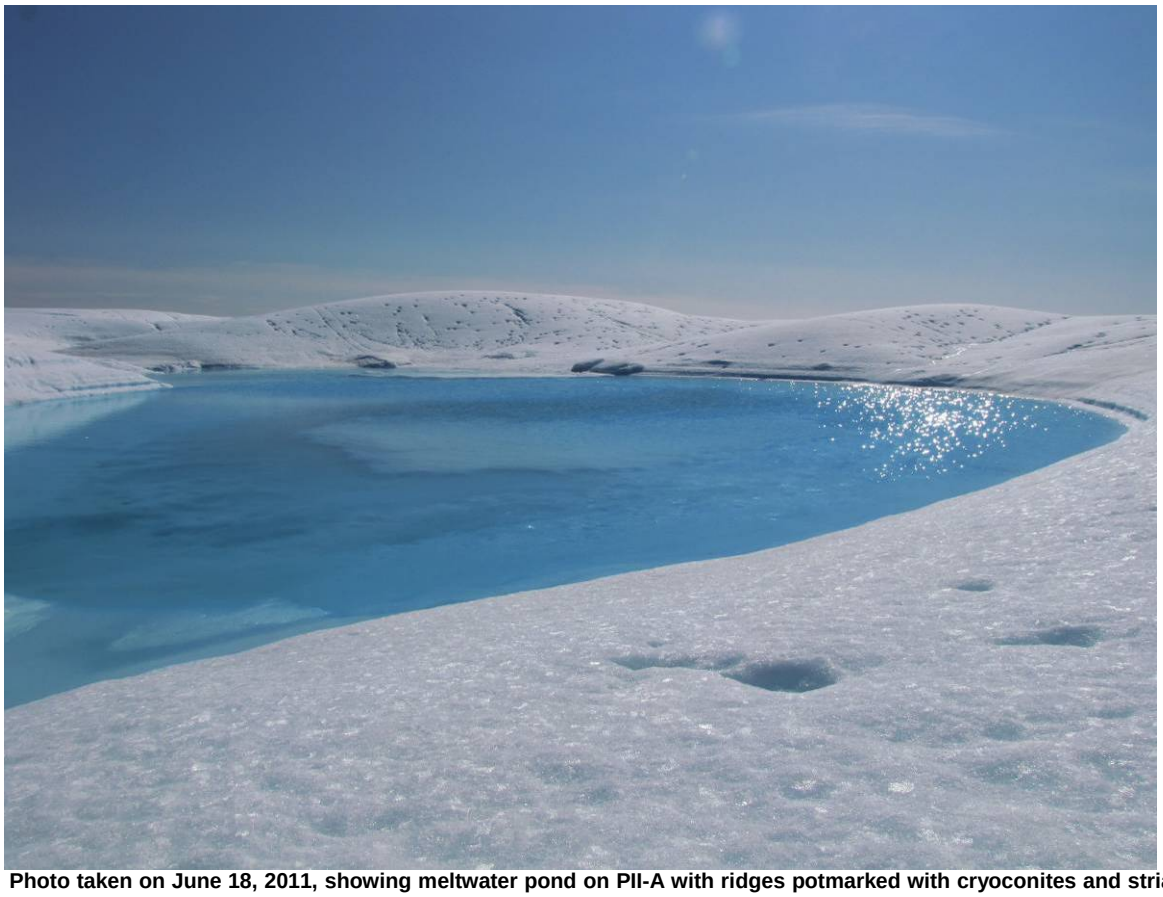

Figure 9. Photo taken on June 18, 2011, showing meltwater pond on PII-A with ridges potmarked with cryoconites and striations in the background; the foreground shows the ice surface texture.

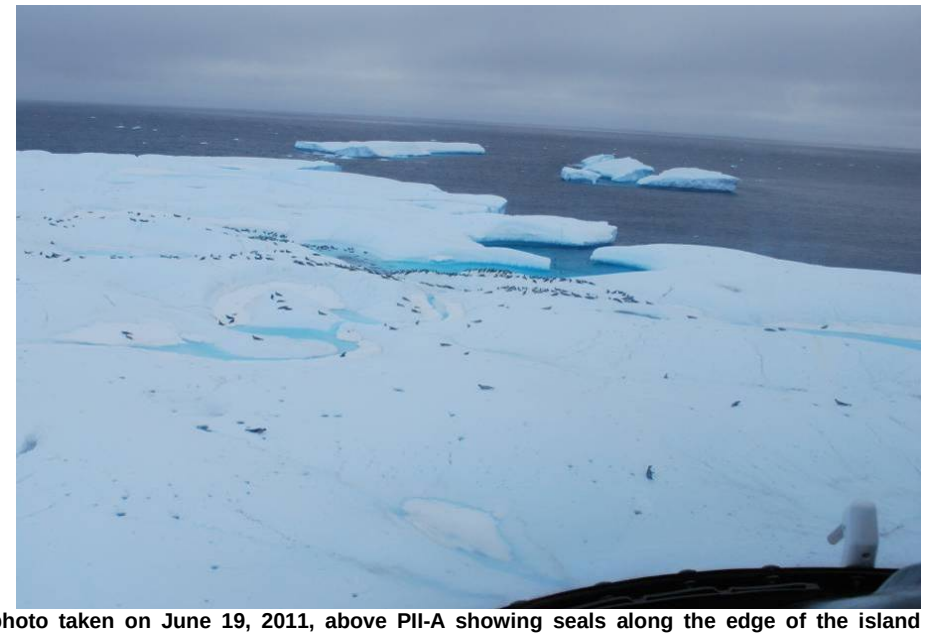

Figure 10. Aerial photo taken on June 19, 2011, above PII-A showing seals along the edge of the island and icebergs in the background that had shed from its perimeter.

Figure 11. Photo taken on June 17, 2011, showing ridges on ice island PII-A-a in the background with equipment in the foreground for scale.

Discussion and Interpretation

Thickness and Melt Rates.

The thickness of PII-A varied across its length, with the thickest end at Station 3 reaching 81 m and thinning to 48.3 m at Station 8 (Figure 4). The change in thickness along its length reflected the proximity to glacial ice source when the ice was still attached (i.e., thickest end closest to the source; Figure 12). The maximum amount of melt experienced by PII-A during the 35 days between field observations was 4.0 m, a combination of 1.65 m surface melt and 2.3 m bottom melt at Station 4. The minimum amount of recorded melt was 1.9 m at Station 1, which comprised 1.7 m surface melt and 0.2 m bottom melt. Station 1 was situated at the thinner, source-distal end of the ice island (Figure 7), and was < 1.5 km away from the islands edge. The least amount of bottom melt (0.2 m) occurred at the thinner end of the ice island, at a location relatively close to its perimeter. Possible causes for local variability in melt rates may include variations in topography (e.g., the presence or absence of ridges and troughs), as well as the shape of the bottom of the ice island. For example, depressions may exist on the base of the island that focus seawater thereby accelerating melt within the channel walls. However, more data is required to make meaningful conclusions regarding the observed differences in melt rate.

The measured thickness of PII-A from GPR and seismic reflection methods at Station 4 were within 2.5 m of each other (Figure 4, Table 1). This lends a degree of confidence in the ability of both survey systems to accurately identify the base of the ice island. In terms of practicality in the field, the GPR system was far more maneuverable, took up less space and weighed considerably less (~5 kg for the GPR system, compared to ~50 kg for the seismic system). The small size and weight of a system is important for aircraft work as it enables the helicopter to take on more fuel and travel longer distances while potentially carrying more passengers. For point measurements of ice thickness the GPR system is the tool of choice in comparison to the seismic reflection system. The seismic reflection system would be better suited to more detailed studies of the internal structure and profile of such an ice island. In this study, seismic data show a high-amplitude, continuous reflection at 38 ms, originating from within PII-A (Figure 6). This reflection event represents a change in acoustic impedance within the ice island, which suggests a change in the physical properties of the ice. More seismic measurements would allow for this feature to be mapped and in turn provide more detailed information about PII-A's structure.

At the time of both June and July surveys, PII-B was situated in Baffin Bay. Knowing the thickness of PII-A provides indirect information about PII-B. Since PII-B was closer to land and the ice source (Figure 12), its minimum thickness is at least that of the thickest end of PII-A, from which it separated (~81 m if assuming the same melt rate of PII-A). Like PII-A, PII-B would increase in thickness along its length in the direction of ice-source. It is plausible that it could have had a total

thickness of closer to 100 m. (Crawford et al., 2012) show that Berghaus, an ice island fragment likely originating from PII-B, was 124.1 m thick in July 2011; PII-B was 73.1 m thick in October 2011.

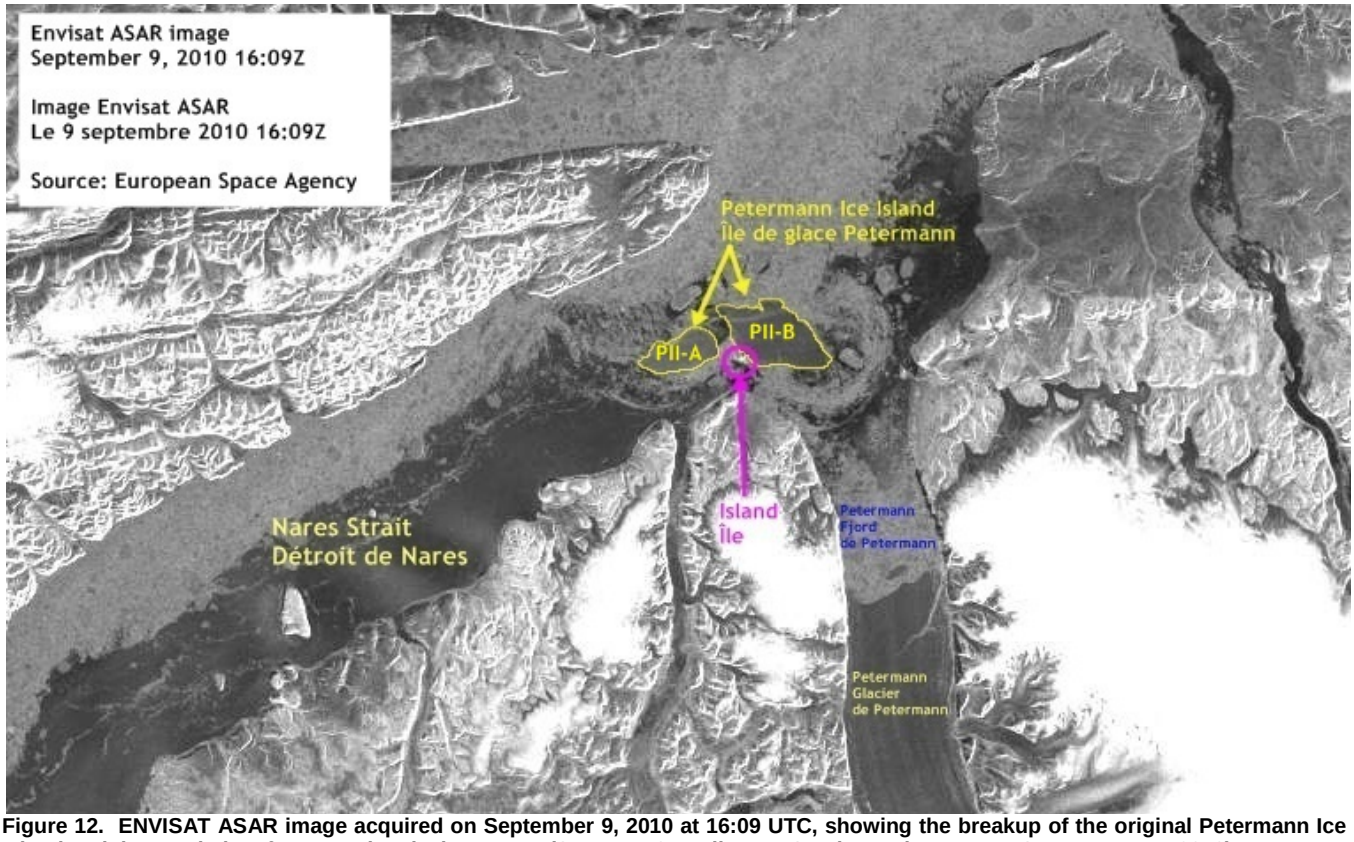

Figure 12. ENVISAT ASAR image acquired on September 9, 2010 at 16:09 UTC, showing the breakup of the original Petermann Ice Island and the proximity of PII-B to the glacier source (Sources: Canadian Ice Service and European Space Agency, 2010).

Implications for Offshore Activities.

Based on an average thickness of 62 m for PII-A measured using GPR, and an area of 62 km^2 determined on June 20th, 2011, using satellite imagery, the mass of PII-A at the time of the survey was approximately 3.5 billion tones. Ice management of a 3.5 billion tonne ice island away from offshore structures may theoretically be possible (i.e., with enough horsepower delivered through numerous large vessels and proper netting), putting it into practice would be logistically very challenging. Upstream ice management strategies might therefore be preferred to deal with such a large mass. These could include accelerating the melt of the ice island with use of surface additives (e.g., carbon black, coal dust) that would enhance the likelihood of it breaking into a number of smaller, more manageable fragments. This technique is referred to as 'dusting' and has been used to weaken river ice prior to breakup operations in North America, Asia and Europe (Haehnel, 1998). Dusting an ice island may be an effective method to accelerate its breakup. However the challenge then would become dealing with numerous smaller ice fragments as opposed to one large one, thereby increasing the risk while reducing the consequences, not to mention the time and cost of ice management activities.

Concluding Remarks and Recommendations

As resource exploration moves into the high latitudes a new set of challenges arise. One such challenge is large masses of ice, namely ice islands, inhabiting the waters around offshore infrastructure. Since 2010 the Petermann Glacier has shed two large islands from its foot, a 253 km^2 fragment in 2010 and more recently a 130 km^2 fragment in July 2012. The 2012 ice island has since broken into several km-scale pieces that are drifting south (Fuglem et al., 2012). Within the last decade, at least 16 smaller ice islands (<0.5 km long and wide) were observed on the Grand Banks (C-CORE, 2011). To mitigate the risks associated with these large ice masses, more knowledge of their physical properties and environmental behavior is required to enable development of appropriate ice island management strategies. This information can be obtained through fieldwork on ice islands, such as that presented in this study, but also from fieldwork and satellite image analysis (particularly using SAR imagery) of ice while it is still attached to the glacier. Identification of fractures and possible calving locations could provide inputs to models and the ability to plan for potential ice island impacts in downstream locations. Model studies of melt rate and drift behavior of large ice islands in relation to sea state, sea and air temperature, such as that presented by (Fuglem et al., 2012), could also help in understanding the 'ice risk factor' inherent to offshore exploration activities in high-latitude regions.

Acknowledgements

We would like to thank Canadian Helicopters and the Captain and crew of CCGS Amundsen for their support and professionalism during the collection of geophysical and other data. Special thanks to pilot Dean Burry for his help in the field and for getting us safely to and from the ice islands. Derry Nichol, Joshua Barnes and Gerry Piercey are gratefully acknowledged for their help in fieldwork planning and logistics. Provincial Airlines and the Canadian Coastguard are recognized for their help in tracking and observations of the Petermann Ice Islands. Globe *Claritas* are acknowledged for donation of their seismic data processing software. Financial support for this work was provided by Canada Foundation for Innovation and Ontario Research Fund.

References

Agency, C.S., 2011. RADARSAT-1 Image. In: M.G.S. Inc (Ed.). MDA Geospatial Services Inc.

Allen, J. and Simmon, R., 2010. Ice Island Calves off Petermann Glacier [ONLINE], Available at: http://www.nasa.gov/topics/earth/features/petermann-calve.html.

Box, J.E. and Decker, D.T., 2011. Greenland marine-terminating glacier area changes: 2000-2010. Annals of Glaciology, 52(59): 91-98.

C-CORE, 2011. Ice Island R&D Program, Proposal P-11-056. C-CORE, St. John's, NL.

Crawford, A. et al., 2012. Improvements to Iceberg Drift and Deterioration Models for Use with Ice Islands in the Eastern Canadian Arctic, International Polar Year (IPY), Montreal, QC.

Falkner, K.K. et al., 2011. Context for the recent massive Petermann Glacier calving event. EOS Transactions, American Geophysical Union, 92(14): 117-118.

Fuglem, M., Richard, M., Kennedy, A., King, T. and Cater, N., 2012. Modelling Risks to Offshore Facilities Associated with Ice Islands off Canada's East Coast, Icetech, Banff, Alberta.

Haehnel, R.B., 1998. Nonstructural Ice Control. US Army Corps of Engineers, Cold Regions Research and Engineering Laboratory, pp. 43.

LLC, M.G., 2012. Drifting Buoy 47557. Available at: http://www.sailwx.info/shiptrack/shipdump.phtml?call=47557, Seattle.

Macheret, Y.Y., Moskalevsky, M.Y. and Vasilenko, E.V., 1993. Velocity of Radio-Waves in Glaciers as an Indicator of Their Hydrothermal State, Structure and Regime. Journal of Glaciology, 39(132): 373-384.

Narod, B.B. and Clarke, G.K.C., 1994. Miniature High-Power Impulse Transmitter for Radio-Echo Sounding. Journal of Glaciology, 40(134): 190-194.

Nick, F.M. et al., 2012. The response of Petermann Glacier, Greenland, to large calving events, and its future stability in the context of atmospheric and oceanic warming. Journal of Glaciology, 58(208): 229-239.

Service, C.I. and Canada, M.S.o., 2005. MANICE, Manual of Standard Procedures for Observing and Reporting Ice Conditions. Government of Canada, Ottawa, Ontario.